Pergamon

Available online at www.sciencedirect.com
SCIENCE DIRECT®

Cement and Concrete Research 34 (2004) 495–505

CEMENT AND CONCRETE RESEARCH

Macroscopic model of concrete subjected to alkali–aggregate reaction

M.C.R. Farage*, J.L.D. Alves, E.M.R. Fairbairn

Department of Civil Engineering, COPPE—Universidade Federal do Rio de Janeiro, Cidade Universitária, Ilha do Fundão, CP 68506, CEP 21945-970, Rio de Janeiro, RJ, Brazil

Received 10 April 2003; accepted 4 September 2003

Abstract

The structural behaviour of concrete affected by alkali–aggregate reaction (AAR) is difficult to model due to the amount of random parameters that govern this chemical process. The aim of this work is to present a macroscopic approach whose main features are the consideration of uncoupling between AAR and stress and the representation of the anisotropic characteristic of chemical swelling. Experimental results concerning reactive concrete samples were simulated to verify whether the model was capable of describing the behaviour of affected structures under certain loading and boundary conditions. Loading–unloading response was also considered to simulate the effect of joints opening, which is a commonly used technique for releasing AAR generated stresses in affected structural elements. The obtained results were compared to test data and showed good agreement.

Keywords: Crack detection; Alkali–aggregate reaction; Finite element analysis; Modeling; Smeared cracking

1. Introduction

1.1. General aspects of AAR expansion

Structural problems related to alkali–aggregate reaction (AAR) have been detected in concrete structures since the beginning of the 20th century, but it was not before 1940 that it was first identified by Stanton [27]. Since then, many efforts have been made to minimize its deleterious effects on concrete. Gel exudation, swelling and cracking are often associated with AAR development. Any kind of concrete structure may be affected, although structures in direct contact with water, such as dams and bridges, are particularly susceptible to AAR development, given that moisture conditions play an important role in this chemical process [3]. Presently, the only way to obtain AAR safe concrete [4,11,23,26] is by identifying the potential reactivity of aggregates and/or adding pozzolanic admixtures to the material. Nevertheless, a great number of operating structures made of reactive concrete still constitute a matter of concern. As in most cases, it is impossible to interrupt AAR, the only way to lessen its harmful effects is by taking remedial measures whose effectiveness depends strongly on an adequate prediction of the stress and strain field development.

AAR depends on the availability of three factors: alkalis liberated from cement during hydration, siliceous minerals present in certain kinds of aggregates and water [6,7,18,27]. Several microscopic and random factors are involved in AAR expansion, such as concrete porosity, amount and location of reactive regions in the material and permeability [18–20,22,24]. These parameters, added to concrete's intrinsic heterogeneity, turn simulating AAR expansion into a rather complex task. Even though AAR process has not been well explained so far [18,27], the commonly accepted theory for describing it is the one proposed by Glasser and Kataoka (cited in Ref. [8]), under which there are two distinct phases to be considered: gel formation and water absorption by the gel, causing expansion. According to this mechanism, reaction does not always lead to expansion. As long as there is enough void space to be filled by the gel—pores and cracks—concrete volume remains unchanged.

1.2. Stress influence and anisotropic behaviour

It is well known that stresses influence the reaction kinetics [1,13,27]. Nevertheless, because of the lack of experimental information concerning this subject, knowl-

* Corresponding author. Rua Antônio Altaf, 86/601, CEP 36033-330, Juiz de Fora, MG, Brazil.
E-mail address: farage@coc.ufrj.br (M.C.R. Farage).

0008-8846/$ – see front matter © 2004 Elsevier Ltd. All rights reserved.
doi:10.1016/j.cemconres.2003.09.001

edge of the chemical–mechanical coupling is yet unsatisfactory. Experimental results obtained from a laboratory research conducted at the Laboratoire Central des Ponts et Chaussés (LCPC, Paris, France) points to the possibility that chemical–mechanical uncoupling may be assumed for specific loading and boundary conditions [22]. According to the tests performed by Larive, the anisotropic characteristic of AAR expansion is noticed even in unloaded conditions, deriving from many local factors that may affect cracking formation, for instance, concrete porosity, tensile strength variation and aggregate distribution. Such characteristic, though, is much more evident in the presence of loading. By comparing uniaxially loaded concrete cylindrical samples with unloaded ones, it is noted that chemical expansion is negligible in the loading direction, whereas transverse (diametric) variation is significantly increased. Total volumetric variation, consequently, remains almost the same under free expansion and loading conditions. The observed behaviour takes place under stresses up to about 30% of concrete compressive strength. Higher stresses cause concrete to undergo extensive cracking, which opens enough space for the gel without resulting in concrete expansion.

1.3. Loading–unloading response

AAR expansion may cause serious damage in operating structures. For instance, in dams there are records of operational problems due to closing of expansion joints and changing of the original geometry of structural components. A frequently used remedial technique is opening or reopening of expansion joints [1,9,29] to release the generated stresses and allow the original geometry to be recovered. Larive [22] provides detailed information about this subject, which was taken as a reference for calibrating the adopted postcracking constitutive model [15]. A brief description of the reported unloading response of AAR-affected concrete samples, initially subjected to uniaxial loading, follows:

- Under external compression, AAR expansion manifests mainly in free directions.
- In case of unloading occurring during gel production, AAR expansion develops as if loading had never been applied.

Considering the above information, numerical simulations have been performed aiming to reproduce the observed experimental behaviour.

2. Proposed model

2.1. Main assumptions

The proposed model [14] is based on the following assumptions: uncoupling between stress and AAR gel formation; anisotropic behaviour represented by means of a smeared crack approach. As a simplification, free expansion was considered as isotropic. Reaction kinetics is given as input data representing the gel expansion evolution in relation to time.

2.2. Constitutive model

2.2.1. One-dimensional model

The analogue model shown in Fig. 1 illustrates the simple but effective assumed mechanism and helps explain the assumptions considered in this work. It was developed based on the elastic model proposed by Ulm et al. [28] and further enhanced [14] to allow cracking of the concrete skeleton.

According to Ulm et al.'s model, concrete is considered as a porous medium comprising a solid matrix skeleton with gel occupying the voids, giving way to the concept of total stress (σ) acting on a unit volume of concrete and gel, effective stress (σ_μ) acting on the solid matrix and pore pressure (p_g) in the gel. The analogue for AAR gel and concrete behaviour is twofold: one models gel while the other models concrete solid matrix. Gel analogue comprises an expansion cell in series with a linear spring, respectively, representing AAR gel expansion (ε_{ch}) and gel compressibility.

In the present work, we have modified the analogue for concrete by adding a cohesive joint element for modeling crack opening in tension, represented by the concrete tensile strength (σ_t), as shown in the illustrative diagram found in Fig. 1.

According to the proposed model, gel pressure p_g is given by Eq. (1),

$$p_g = E_g(\varepsilon_{ch} - \varepsilon) \tag{1}$$

where ε_{ch} is the AAR-induced strain, ε represents the concrete skeleton strain and E_g is the gel elastic modulus.

The gel-induced pressure p_g is balanced by the stresses originating in the concrete skeleton σ_μ, and, in case of existing loadings or depending on boundary conditions, also

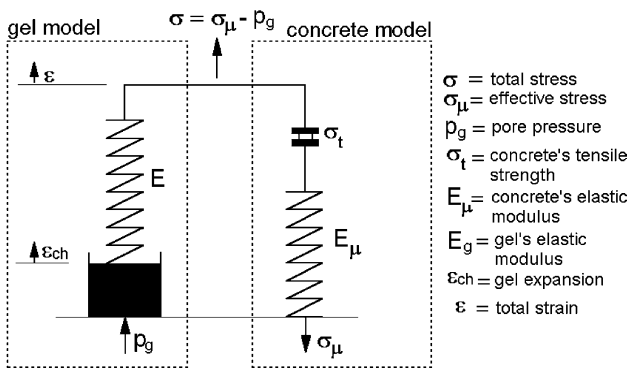

Fig. 1. One-dimensional model of expansive concrete behaviour.

by external stresses, causing the system equilibrium to be described by Eq. (2).

$$\sigma = \sigma_\mu - p_g \tag{2}$$

The material total strain ε is the superposition of elastic strain (ε^e) and postcracking strain (ε_{cr}), as indicated in Eq. (3).

$$\varepsilon = \varepsilon^e + \varepsilon_{cr} \tag{3}$$

2.2.2. Smeared crack model

Cracking was modeled within the framework of the classic theory of smeared crack finite element approach, with no decomposition of total strain variation into its intact (uncracked) and damaged (cracked) contributions [16,17]. Cracking state is represented by total strain in a homogeneous manner, by replacing the material's elastic isotropic matrix for an anisotropic one, which introduces degradation in the system.

By taking as reference a three-orthogonal system (n–s–t) local to a formed crack, where n is normal to the crack plane and s and t belong to the crack plane, stress–strain relationship is given by Eq. (4).

$$\begin{Bmatrix} \sigma_n \\ \sigma_s \\ \sigma_t \\ \tau_{ns} \\ \tau_{st} \\ \tau_{tn} \end{Bmatrix} = \begin{bmatrix} D_n & D_{ns} & D_{nt} & 0 & 0 & 0 \\ D_{ns} & D_s & D_{st} & 0 & 0 & 0 \\ D_{nt} & D_{st} & D_t & 0 & 0 & 0 \\ 0 & 0 & 0 & G_{ns} & 0 & 0 \\ 0 & 0 & 0 & 0 & G_{st} & 0 \\ 0 & 0 & 0 & 0 & 0 & G_{tn} \end{bmatrix} \begin{Bmatrix} \varepsilon_n \\ \varepsilon_s \\ \varepsilon_t \\ \gamma_{ns} \\ \gamma_{st} \\ \gamma_{tn} \end{Bmatrix} \tag{4}$$

Nine independent moduli define this three-dimensional relation: D_n, D_s, D_t, D_{ns}, D_{nt}, D_{st}, G_{ns}, G_{st} and G_{tn} [12,16]. These moduli are functions of the material cracking state, following relations that are settled in accordance with the specifics of the considered problem. Similarly to the model proposed by Rashid (1968), cited in Ref. [16], the model presented here assumes that as soon as a crack opens, the material loses its ability of transmitting additional tension forces in the direction normal to the crack surface (n direction). All moduli related to forces in the n direction change gradually, as a function of crack opening, so that the stress–strain relationship expresses the resulting degradation in this direction. For the sake of simplicity, fracture is assumed to propagate only in Mode I, which in classical fracture mechanics approach states that crack opening and propagation is controlled only by tensile/compressive stresses normal to the crack surface.

The adapted smeared crack model derives from the concept of cohesive cracking proposed by Hillerborg et al. [21], integrated to the crack band model presented by Bazant and Oh [5]. The energy release rate G_f is an intrinsic parameter that governs crack opening in concrete. This parameter is the energy required to crack a unitary area of the material and is represented by the material's stress–displacement relationship, from which the stress–strain relationship is obtained through a characteristic width h, which is a region of the finite element where crack opening is considered to process.

2.2.3. Crack orientation

The fixed orthogonal crack model was adopted. This model limits the number of cracks at a point according to the number of normal stress components of the considered problem (three in three-dimensional, plane strain and axisymmetric cases and two in plane stress problems, for example). No matter how many cracks there are at a point, their faces are assumed to be normal to each other [25].

2.2.4. Cracking detection

Rankine criterion [12] was chosen as a cracking detection surface—a crack forms when maximum principal stress reaches the concrete tensile strength. Crack surface is taken as normal to the principal stress direction. In a three-dimensional problem, as soon as a crack is detected in a certain element, the direction normal to the crack surface is considered as uncoupled to the other directions, which are still intact and coupled among them.

2.2.5. Postcracking constitutive relation

Cracking is considered to start as soon as Rankine surface is attained. Once an element experiences cracking in a particular direction, subsequent calculations are developed under the consideration of a new basis, set by crack orientation. Stress–strain relationship normal to the crack surface obeys the postcracking behaviour illustrated in Fig. 2, where g_f is the specific energy release rate G_f/h, h is the width of the crack band [5], E is Young's modulus, ε_{crl} is the strain related to limit crack opening, which determines the end of material cohesiveness, and E_{cr} is the postcracking modulus that relates stress to strain in the cracked state.

An inverse analysis was performed [15], taking as a reference experimental data available in Ref. [22], showing

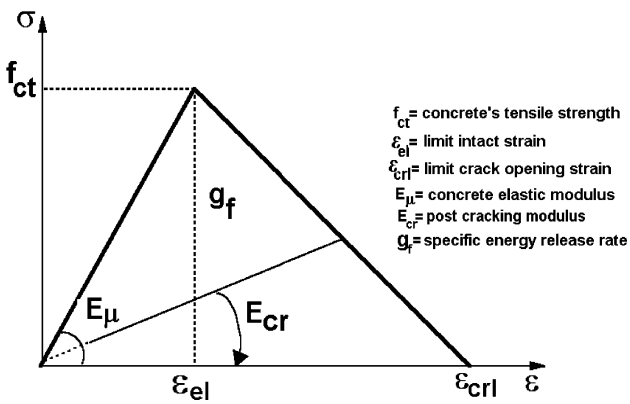

Fig. 2. One-dimensional stress–strain relation.

that the constitutive relationship that best fits reactive concrete in cracked state is the one that considers a region of ductile degradation, as presented in Fig. 3. Cracked reactive concrete is assumed to keep its capability of transmitting forces, with no tensile strength decay, until crack strain reaches a limit value ε_{crl}.

2.2.6. Crack closing/reopening conditions

In a simple manner, cracks are allowed to close and reopen completely, depending on the loading conditions. In spite of residual strain being totally neglected, the model allows the release of cracking energy, which is represented by variations of the material's elastic modulus. In the cracked state, the modulus E_{cr} relates stresses to strains, as illustrated in Fig. 4.

2.3. Reaction kinetics

AAR gel expansion is an input data. Eq. (5), as proposed by Larive [22], was implemented to represent free expansion evolution of reactive concrete.

$$\dot{\varepsilon}_{ch} = \frac{\varepsilon_\infty}{\tau_c} \frac{\left(e^{\frac{T}{\tau_c}} + e^{\frac{-T+\tau_l}{\tau_c}}\right)}{\left(1 + e^{\frac{-T+\tau_l}{\tau_c}}\right)^2} \tag{5}$$

Eq. (5), where T is the time, represents the one-dimensional chemical expansion rate ($\dot{\varepsilon}_{ch}$) as a function of three independent parameters: asymptotic volumetric strain (ε_∞); latency time (τ_l) and characteristic time (τ_c). Such parameters may be identified by adjustments of experimental curves, and express temperature and humidity influence on the reaction development. As isotropic behaviour is assumed for concrete under free expansion, the volumetric chemical expansion rate $\dot{\varepsilon}^V_{ch}$ is represented by Eq. (6).

$$\dot{\varepsilon}^V_{ch} = 3\dot{\varepsilon}_{ch} \tag{6}$$

2.4. Extension to three dimension

For the three-dimensional case, two reference systems are adopted: a global system (x–y–z) and a local system

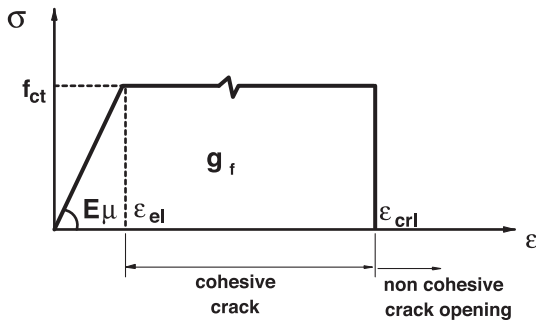

Fig. 3. One-dimensional stress–strain relationship considering ductile postcracking behaviour (see Fig. 2 for definition of symbols).

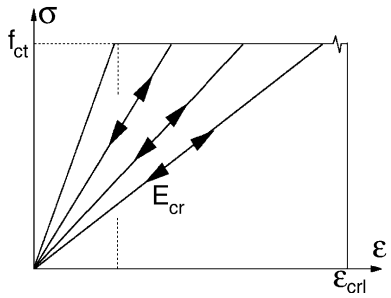

Fig. 4. Crack closing–reopening mechanism: the postcracking modulus E_{cr} is a function of the material's cracking state.

(1–2–3) that is coincident with the principal stress directions. System equilibrium is given by Eq. (7).

$$\boldsymbol{\sigma} = \boldsymbol{\sigma}_\mu - \mathbf{p}_g \tag{7}$$

where pore pressure ($\mathbf{p}_g$) is represented in Eq. (8).

$$\mathbf{p}_g = B \begin{bmatrix} 3\varepsilon_{ch} - \varepsilon_v & 0 & 0 \\ 0 & 3\varepsilon_{ch} - \varepsilon_v & 0 \\ 0 & 0 & 3\varepsilon_{ch} - \varepsilon_v \end{bmatrix} \tag{8}$$

where B is the gel's bulk modulus (Eq. (9)):

$$B = \frac{E_g}{3(1 - 2\nu_g)} \tag{9}$$

where ν_g is the gel's Poisson's ratio, and the volumetric strain (ε_v) is expressed by Eq. (10), valid for small strains:

$$\varepsilon_v = \varepsilon_x + \varepsilon_y + \varepsilon_z \tag{10}$$

That is, the trace of strain tensor where ε_i is strain in direction i ($i = x, y, z$).

2.4.1. Mechanical response to imposed strain increments

Incremental stress–strain relationship is expressed by Eq. (11).

$$\dot{\boldsymbol{\sigma}}_\mu = \mathbf{D}\dot{\boldsymbol{\varepsilon}} \tag{11}$$

A finite element is considered as intact while the stress in the principal stress direction 1 is up to f_{ct} ($\sigma_1 \le f_{ct}$) and, as a consequence, $\varepsilon_1 \le \varepsilon_{e1}$. The elastic matrix $\mathbf{D}$ related to the intact state is represented by Eq. (12):

$$\mathbf{D} = d \begin{bmatrix} 1 & \frac{\nu}{1-\nu} & \frac{\nu}{1-\nu} & 0 & 0 & 0 \\ \frac{\nu}{1-\nu} & 1 & \frac{\nu}{1-\nu} & 0 & 0 & 0 \\ \frac{\nu}{1-\nu} & \frac{\nu}{1-\nu} & 1 & 0 & 0 & 0 \\ 0 & 0 & 0 & \frac{1-2\nu}{2(1-\nu)} & 0 & 0 \\ 0 & 0 & 0 & 0 & \frac{1-2\nu}{2(1-\nu)} & 0 \\ 0 & 0 & 0 & 0 & 0 & \frac{1-2\nu}{2(1-\nu)} \end{bmatrix} \tag{12}$$

where v is the Poisson's ratio of concrete and d is given by Eq. (13).

$$d = \frac{E_\mu(1-v)}{(1+v)(1-2v)} \tag{13}$$

As soon as cracking is detected ($\varepsilon_I > \varepsilon_{el}$, $I = 1$, 2 or 3), directions normal to the crack surfaces are considered as uncoupled to the other directions, since the model does not take shear stresses in the cracked planes into account. The uncoupling is introduced in the system by replacing the initial elastic matrix $\mathbf{D}$ by $\mathbf{D}_{cr}$ [Eq. (14)], in which all terms related to direction couplings are null. The model allows a maximum number of three cracks per element and, from crack formation on, calculations are made in the local reference system (1–2–3).

$$\dot{\boldsymbol{\sigma}}_I = \mathbf{D}_{cr}\dot{\varepsilon}_I \qquad I = 1,2,3 \tag{14}$$

where $\dot{\boldsymbol{\sigma}}_I$ is the stress rate and $\dot{\varepsilon}_I$ is the total strain rate in direction I, $I = 1$, 2, 3.

The matrix $\mathbf{D}_{cr}$ represents the material degradation state and the assumed uncoupling of the "cracked" directions, as follows.

- *One crack:* The element presents one crack if the following conditions are observed: $\varepsilon_1 > \varepsilon_{el}$; $\varepsilon_2 \le \varepsilon_{el}$ and $\varepsilon_3 \le \varepsilon_{el}$. Direction 1 is then considered as uncoupled and the stress–strain relationship in this direction obeys the one-dimensional postcracking behaviour described by Fig. 3, whereas directions 1 and 2 remain coupled. Matrix $\mathbf{D}_{cr}$ related to this condition is given by Eq. (15).

$$\mathbf{D}_{cr} = \begin{bmatrix} E_{cr} & 0 & 0 & 0 & 0 & 0 \\ 0 & d & \frac{v}{1-v}d & 0 & 0 & 0 \\ 0 & \frac{v}{1-v}d & d & 0 & 0 & 0 \\ 0 & 0 & 0 & 0 & 0 & 0 \\ 0 & 0 & 0 & 0 & \frac{1-2v}{2(1-v)}d & 0 \\ 0 & 0 & 0 & 0 & 0 & 0 \end{bmatrix} \tag{15}$$

where E_{cr} is the postcracking modulus, defined in Fig. 2.

- *Two cracks:* A finite element presents two cracks if $\varepsilon_1 > \varepsilon_{el}$; $\varepsilon_2 > \varepsilon_{el}$ and $\varepsilon_3 \le \varepsilon_{el}$. In this case, all three directions are considered as uncoupled and the problem is reduced to three one-dimensional relationships: postcracking relationship is assumed for the incremental stress–strain relationships in directions 1 and 2, whereas the intact relationship remains for direction 3. Matrix $\mathbf{D}_{cr}$ is then given as Eq. (16).

$$\mathbf{D}_{cr} = \begin{bmatrix} E_{cr} & 0 & 0 & 0 & 0 & 0 \\ 0 & E_{cr} & 0 & 0 & 0 & 0 \\ 0 & 0 & E_\mu & 0 & 0 & 0 \\ 0 & 0 & 0 & 0 & 0 & 0 \\ 0 & 0 & 0 & 0 & 0 & 0 \\ 0 & 0 & 0 & 0 & 0 & 0 \end{bmatrix} \tag{16}$$

- *Three cracks:* A finite element presents three cracks when $\varepsilon_1 > \varepsilon_{el}$; $\varepsilon_2 > \varepsilon_{el}$ and $\varepsilon_3 > \varepsilon_{el}$. The three principal

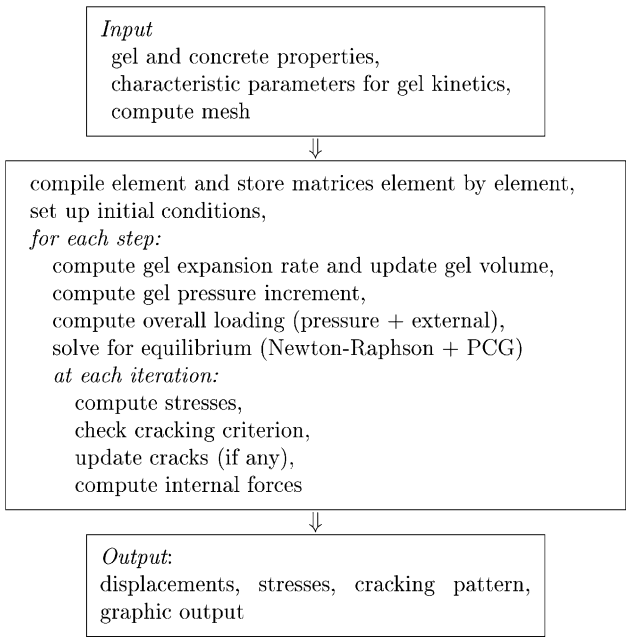

Fig. 5. Diagram representing the main aspects of the implementation.

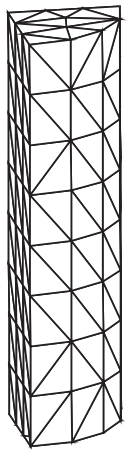

Fig. 6. Finite element mesh for 1/4 of the concrete sample.

directions are then considered as uncoupled and matrix $\mathbf{D}_{cr}$ is represented as Eq. (17).

$$\boldsymbol{D}_{cr} = \begin{bmatrix} E_{cr} & 0 & 0 & 0 & 0 & 0 \\ 0 & E_{cr} & 0 & 0 & 0 & 0 \\ 0 & 0 & E_{cr} & 0 & 0 & 0 \\ 0 & 0 & 0 & 0 & 0 & 0 \\ 0 & 0 & 0 & 0 & 0 & 0 \\ 0 & 0 & 0 & 0 & 0 & 0 \end{bmatrix} \quad (17)$$

3. Implementation

The model was implemented in a reference program developed in FORTRAN for nonlinear analysis of three-dimensional problems via finite element method [2] through four-node tetrahedral elements. The resulting system of nonlinear equations is solved by a Newton–Raphson iterative-incremental technique. The initial stiffness matrix is used as an approximation for the discrete Jacobian and kept constant throughout the analysis. The solution of the linearized system uses the preconditioned conjugated gradient (PCG) method, which was implemented under an element-by-element (EBE) technique avoiding global stiffness matrix assemblage and factoriza-

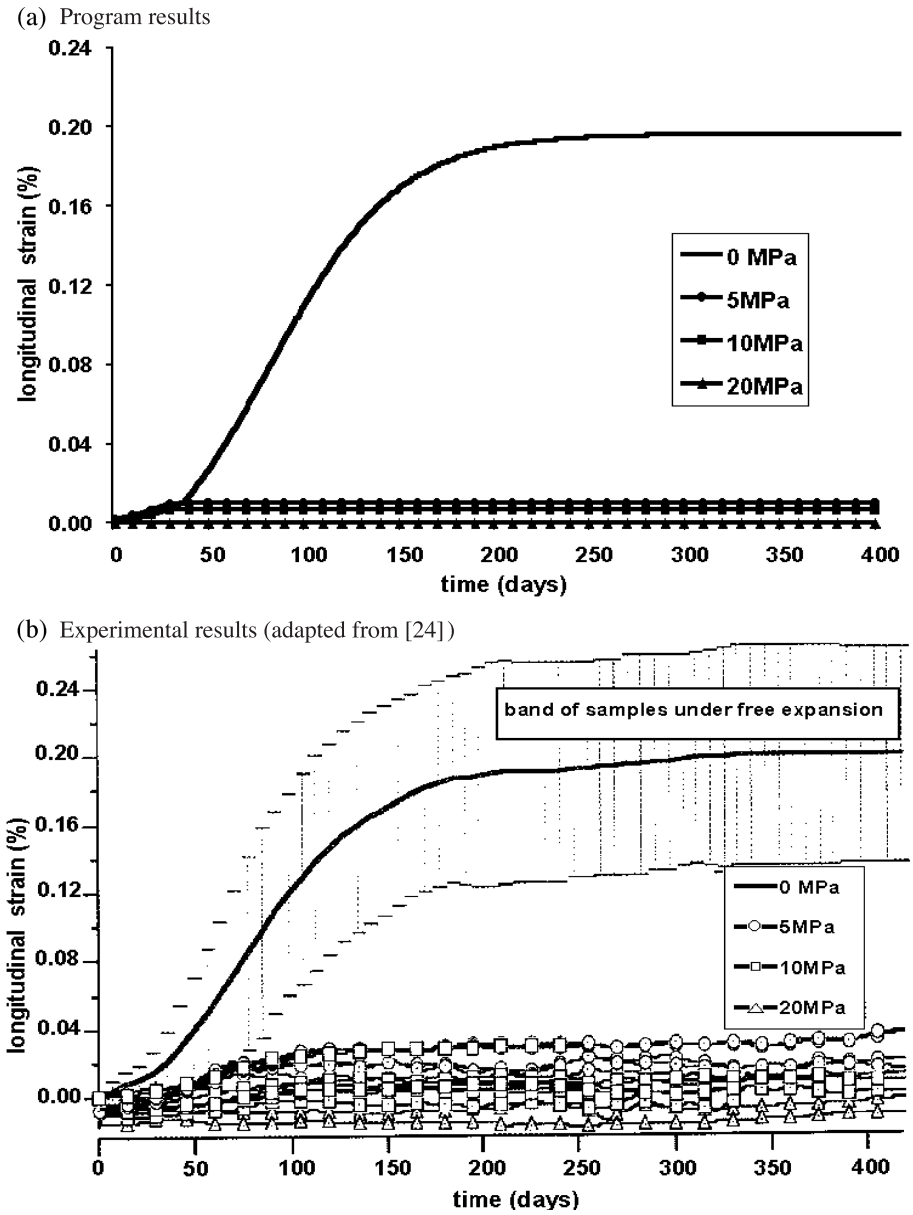

Fig. 7. Longitudinal strain due to AAR × time relationship.

tion [10]. For the material, it was considered nonlinear behaviour under tension by the adoption of the smeared cracking model, taking Rankine criterion for crack detection. Postcracking calculations are made on a new basis, determined by crack directions, which requires bookkeeping of the directions of principal stresses related to the instant of crack initiation. Fig. 5 illustrates the main aspects of the implementation.

4. Numerical simulations

4.1. Reactive concrete samples

This example aims to demonstrate the adequacy of the proposed model by reproducing the laboratory tests performed by Larive [22] on cylindrical samples made of reactive concrete subjected to constant uniax-

(a) Program results

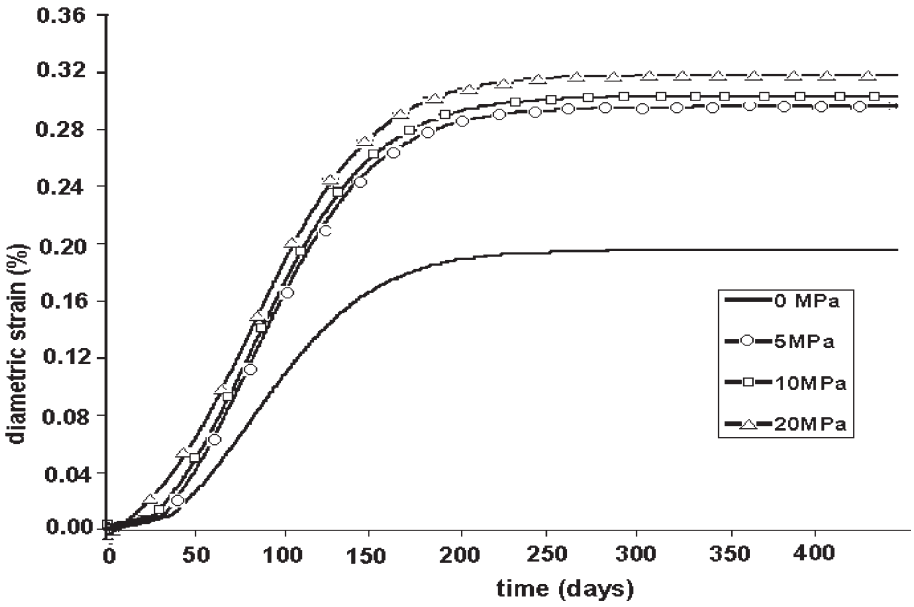

(b) Experimental results (adapted from [24])

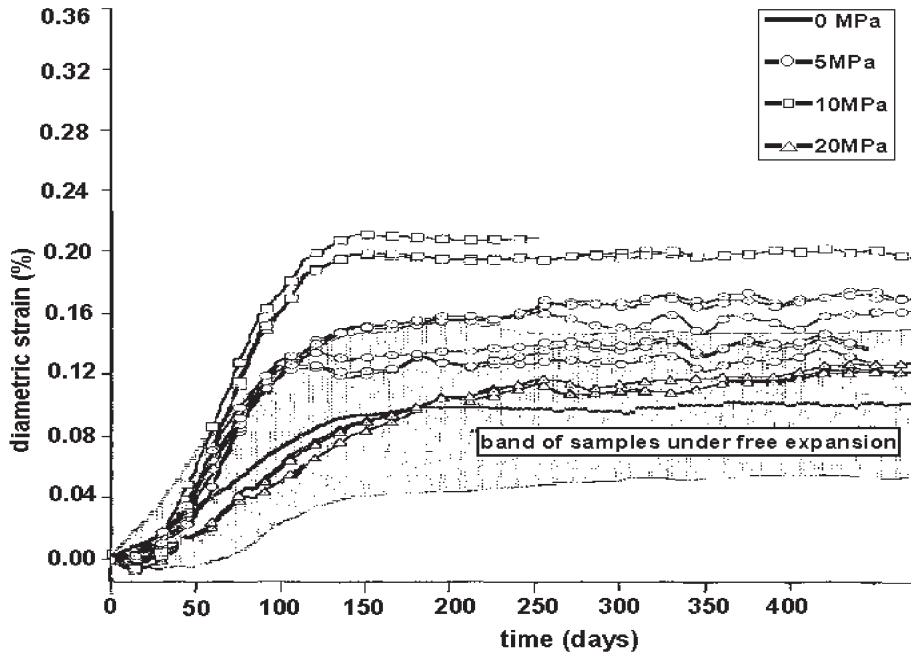

Fig. 8. Diameter variation due to AAR × time.

(a) Program results

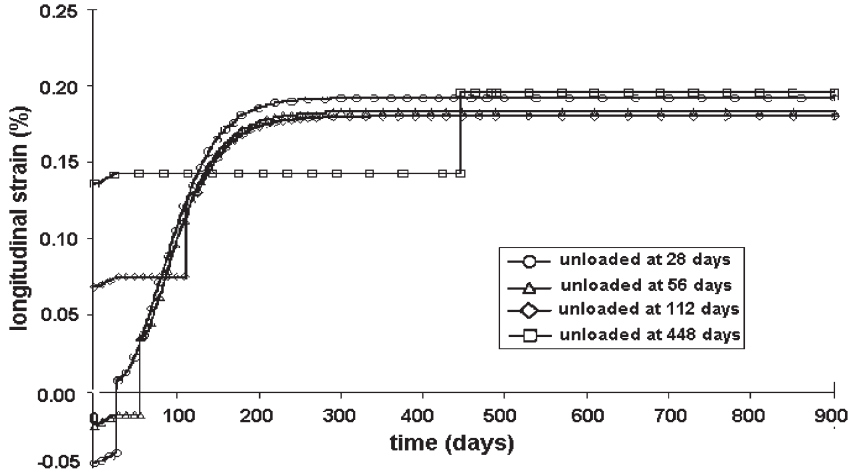

(b) Experimental results (adapted from [24])

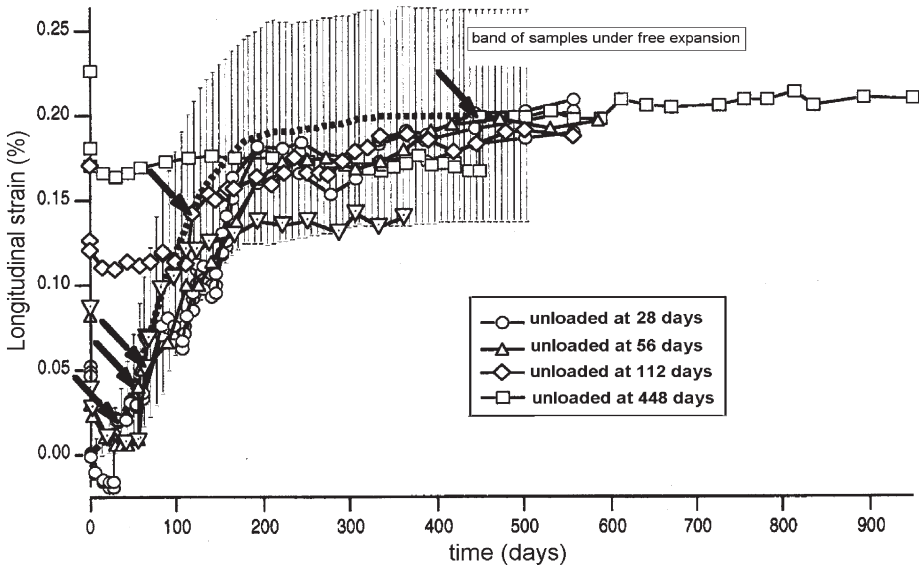

Fig. 9. Post unloading behaviour.

ial compressive loading and to loading–unloading conditions.

The reaction kinetics is given by Eq. (5), considering a temperature of 38 °C. The related characteristic parameters were obtained from Ref. [22]: $\tau_1 = 82.5$ days, $\tau_c = 33.4$ days and $\varepsilon_\infty = 0.196\%$. The assumed concrete properties were the same as those of the tested samples [22]: $E_\mu = 1.82 \times 10^4$ MPa, $\nu = 0.23$, $f_c = 35$ MPa and $f_{ct} = 3.5$ MPa. In the absence of specific data for gel characterisation, it was assumed $E_g = 1.82 \times 10^4$ MPa and $\nu_g = 0$. By inverse analysis, the numeric response for concrete under free expansion was then adjusted to represent the experimental free expansion curve.

The computational mesh shown in Fig. 6 exploits the symmetry of the problem by modeling 1/4 of the cylindrical specimen, using 108 nodes and 288 tetrahedral elements.

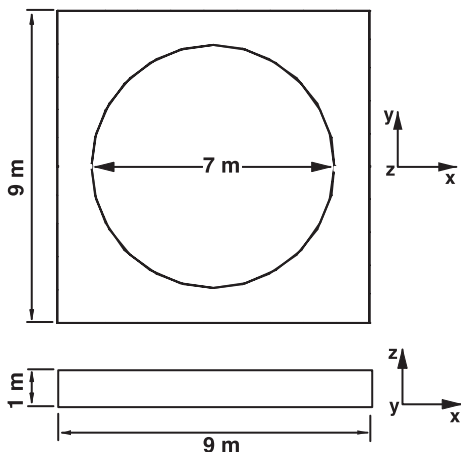

Fig. 10. Discharge ring model characteristics.

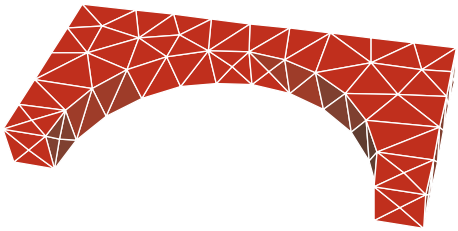

Fig. 11. Discharge ring mesh.

4.1.1. Constant uniaxial loading

Uniaxial compressive loadings relative to 5, 10 and 20 MPa were applied to a cylindrical sample to simulate test conditions. Numeric free expansion curves were also obtained. Longitudinal strain evolution and diameter variation were obtained via the developed program and compared to the experimental data, as one can see in Figs. 7 and 8, respectively.

The experimental behaviour, represented in Figs. 7(b) and 8(b) indicates that the uniaxial loading prevents the strain development in the loading direction. Such strains are almost completely transferred to the free directions, as the curves related to 5 and 10 MPa indicate. Under 20 MPa, such strain transferring is not complete due to the intense cracking, which has a reducing effect on the chemical induced expansion by allowing release of the gel.

As a whole, the numeric results related to the samples under 5 and 10 MPa [shown in Figs. 7(a) and 8(a)] prove that the proposed model is able to reproduce the loading induced anisotropy for uniaxial stresses up to 30% of the concrete compressive strength. It is noticed in Fig. 8 that the calculated values were higher than those obtained in laboratory due to the assumption of isotropic behaviour for concrete under free expansion, as a simplification. The reducing effect observed in the sample under 20 MPa was not considered in the model because it depends on the incorporation of plasticity effects in the program.

(a) Ovalization after 4 years of AAR exposure (upper and bottom edges restrained)

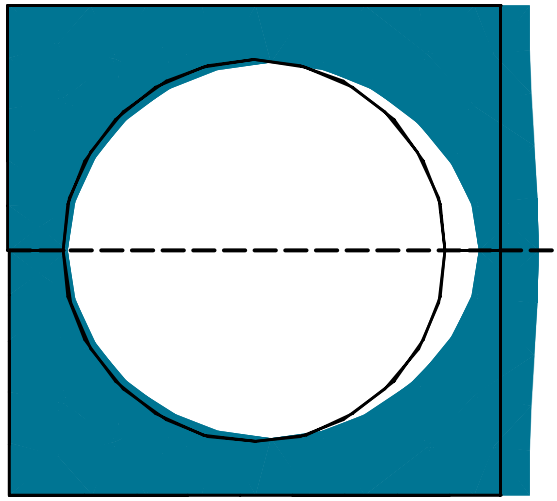

(b) Configuration due to joints opening (upper and bottom edges released)

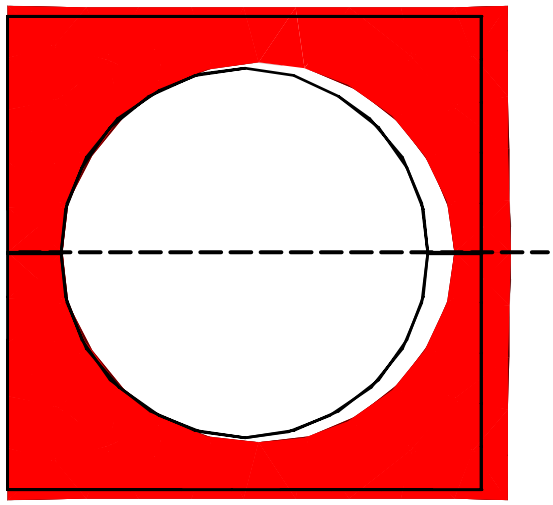

Fig. 13. Effect of early joint opening (magnification factor of 500).

(a) Initial boundary conditions (upper and left edges restrained)

(b) Joint opening (upper edge free to expand)

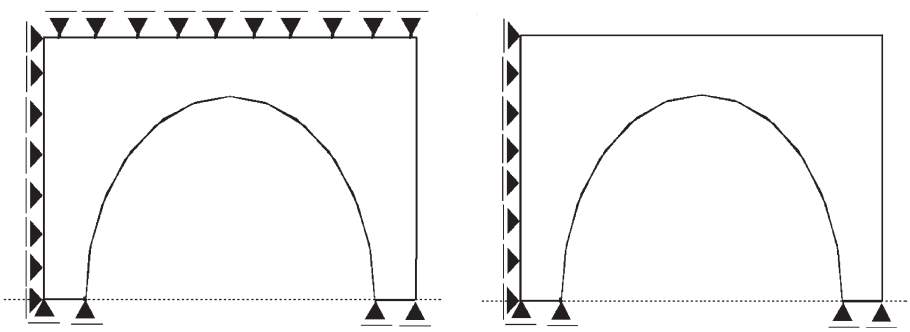

Fig. 12. Simulated execution of joint opening by changing of boundary conditions.

4.1.2. Loading–unloading behaviour

The reactive concrete sample was first subjected to longitudinal loading relative to uniaxial stresses of 5 MPa and later unloaded at different periods of time. The longitudinal strain–time relationship was achieved for every unloading condition and compared to the free expansion curve. To verify whether loading influences AAR evolution, every curve was displaced as to coincide with the one related to free expansion. Fig. 9 provides a comparison between the numeric results (Fig. 9(a)) and experimental data (Fig. 9(b)) reported by Larive [22]. Such comparison shows that the implemented model agrees with the experimental behaviour.

4.2. Discharge ring

The aim of this application is to simulate the AAR effect of joints opening on the geometry of a discharge ring deformed under AAR. It is possible due to the loading–unloading mechanism considered by the proposed model.

(a) Ovalization after 10 years of AAR exposure (upper and bottom edges restrained)

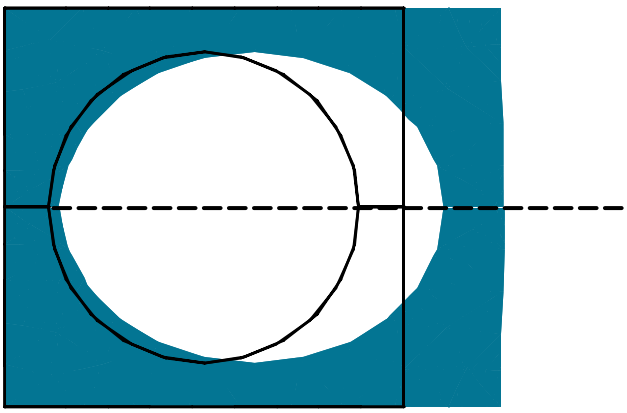

(b) Configuration after joint opening (upper and botttom edges released)

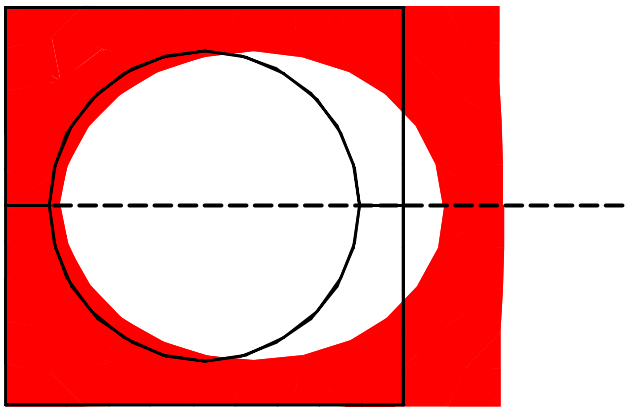

Fig. 14. Effect of late joint opening (magnification factor of 90).

In addition, the developed program allows changing of the original boundary conditions.

The discharge ring is represented by the simplified model illustrated in Fig. 10, considering the symmetry of the problem. The finite element mesh has 96 nodes and 184 tetrahedral elements (Fig. 11). Fig. 12 illustrates the simulation of joint opening by changing the problem's boundary conditions.

AAR development was represented by the gel expansion curve described by Eq. (5), defined by the following characteristic parameters: $\varepsilon_\infty = 0.196\%$, $\tau_l = 3.34$ years and $\tau_c = 8.29$ years. Two unloading situations were simulated: early joint opening, after 4 years of exposure to AAR, when gel expansion was about 10% of ε_∞ and late joint opening, after 10 years of AAR development, when gel expansion was approximately 60% of ε_∞.

4.2.1. Effect of joint opening

Fig. 13 presents the effect of early joint opening on the discharge ring configuration. After 4 years of AAR exposure, the structural element had an oval aspect, shown in Fig. 13(a). The opening of joints allowed the generated stresses to be released and the section regained a nearly circular configuration. At this point most of the finite elements were still intact, making it possible for the structure to recover its original geometry.

In Fig. 14, the effect of late joint opening is illustrated. As one can see in Fig. 14(b) the discharge ring remains oval when joint opening is performed after 10 years of AAR. At that time, all the finite elements presented cracks and the deformations were irreversible.

5. Conclusions

In this paper, a macroscopic AAR model developed within the framework of a smeared crack finite element approach is presented. In spite of several simplification hypotheses, the proposed model was able to simulate laboratory tests performed at LCPC-France [22] concerning reactive concrete samples under constant uniaxial loading. Statistical concepts, such as random distribution of reactive sites, temperature and moisture conditions in the material shall be incorporated to the model [7] to improve the representation of free expansion, which is overestimated herein due to the consideration of isotropic behaviour in the absence of external stresses or restrains [see Fig. 7(a)].

Although simple in essence, the present model is able to reproduce AAR effects in concrete structures under certain loading and boundary conditions, as observed. Comparison between the obtained results and available experimental information shows that the implemented model adequately represents an important feature of AAR-affected concrete—unloading and reloading behaviour. Such an aspect is paramount when considering the usual remedial procedure

adopted in affected massive concrete structures: opening or reopening of expansion joints.

The preliminary results presented herein encourage the application of the developed model to real-world problems. Further studies concerning the coupling between stresses and AAR should be developed to extend the model application to structures under more sophisticated loading and boundary conditions.

Acknowledgements

This work was partially financed by funding from the Coordenação de Aperfeiçoamento de Pessoal de Nível Superior (CAPES), Brasil.

References

[1] L. Adeghe, A. Hindy, M.S. Ho, R.H. Saunders, G.S. Concrete, Growth mitigation project instrumentation and finite element analysis, Proceedings of the Second International Conference on Alkali–Aggregate Reactions in Hydroelectric Plants and Dams, USCOLD, Chatanooga, Tennessee, 1995, pp. 323–342.

[2] J.L.D. Alves, Programa TriMC: Manual de Entrada de Dados, Department of Civil Engineering, COPPE, UFRJ, Rio de Janeiro, 1996 (in Portuguese).

[3] W.P. Andrade Equipe de Furnas, Concretos Massa, Estrutural, Projetado e Compactado com Rolo. Ensaios e Propriedades, Pini, São Paulo, 1997 (in Portuguese).

[4] M. Alasali, V. Malhotra, J. Soles, Performance of various test methods for assessing the potential alkali reactivity of some Canadian aggregates, ACI Mater. J. 88 (36) (1991) 613–619.

[5] Z.P. Bazant, B.H. Oh, Crack band theory for fracture of concrete, ACI Mater. Struct. 16 (93) (1983) 155–177.

[6] B. Capra, J.-P. Bournazel, Modeling of induced mechanical effects of alkali–aggregate reactions, Cem. Concr. Res. 28 (2) (1998) 251–260.

[7] B. Capra, A. Sellier, Mechanical modelling of alkali–aggregate reaction in concrete structures, in: R. de Borst, J. Mazars, G. Pijaudier-Cabot, J.G.M. van Mier (Eds.), Proceedings of the Fracture Mechanics of Concrete Structures, Cachan, France, 2001, pp. 183–190.

[8] B. Capra, J.-P. Bournazel, E. Bourdarot, Modeling of alkali–aggregate reaction effects in concrete dams, Proceedings of the Second International Conference on Alkali–aggregate Reactions in Hydroelectric Plants and Dams, USCOLD, Chatanooga, Tennessee, 1995, pp. 441–455.

[9] P. Caron, R. Tinawi, P. Leger, M. Veilleux, Slot cutting response of compressed concrete structures, in: R. de Borst, J. Mazars, G. Pijaudier-Cabot, J.G.M. van Mier (Eds.), Proceedings of the Fracture Mechanics of Concrete Structures, Cachan, France, 2001, pp. 879–886.

[10] A.L.G.A. Coutinho, L. Landau, N.F. Ebecken, Avaliação de estratégias computacionais para o método dos elementos finitos em computadores vetoriais, Rev. Int. Métodos Numér. Calc. Diseño Ing. 9 (3) (1993) (in Portuguese).

[11] A. Criaud, C. Defossé, Evaluating the reaction of actual compositions of concrete with respect to alkali–aggregate reactions. Preliminary testing at 110 °C and 150 °C, Mater. Struct. 28 (175) (1995) 32–42.

[12] M.A. Crisfield, Nonlinear finite element analysis of solids and structures, John Wiley & Sons, UK, 1997.

[13] D.D. Curtis, Modeling of AAR affected structures using the GROW3D FEA program, Proceedings of the Second International Conference on Alkali–Aggregate Reactions in Hydroelectric Plants and Dams, USCOLD, Chatanooga, Tennessee, 1995, pp. 457–478.

[14] M.C.R. Farage, Modelagem e implementação numérica da expansão por reação álcali–agregado do concreto, DSc thesis, Department of Civil Engineering, COPPE, Universidade Federal do Rio de Janeiro, Rio de Janeiro, 2000 (in Portuguese).

[15] M.C.R. Farage, E.M.R. Fairbairn, J.L.D. Alves, Application of smeared crack model for simulating concrete chemical expansion, Proceedings of Computational Methods in Engineering 2000, Pontificia Universidade Católica do Rio de Janeiro, Rio de Janeiro, (CD-ROM).

[16] E.M.R. Fairbairn, N.C. Menezes, Rapport sur l'Etat de l'Art de l'Application de la Méthode des Elements Finis au Béton Armé, CEBTP, Département Structures, Service d'Etude des Structures, Paris, 1993 (in French).

[17] P.H. Feenstra, R. De Borst, J.G. Rots, A comparison of different crack models applied to plain and reinforced concrete, in: T.G.M. van Mier, J.G. Rots, A. Bakker (Eds.), Proceedings of the Int. RILEM/ESIS Conference: Fracture Process in Concrete, Rock and Ceramics, E&FN Spon, The Netherlands, 1991, pp. 629–638.

[18] C. Ferraris, Alkali–silica reaction and high performance concrete, Report NISTIR 5742, National Institute of Standards and Technology, Gaithersburg, MD, 1995, pp. 1–20.

[19] C. Ferraris, E. Garboczi, F. Davis, J. Clifton, Stress due to alkali–silica reaction in mortars, Proceedings of the Fourth Materials Engineering Conference, ASCE, Washington, DC, 1996, pp. 1379–1387.

[20] P. Grattan-Bellew, Laboratory evaluation of alkali–silica reaction in concrete from Saunders generating station, ACI Mater. J. 92 (2) (1995) 126–134.

[21] A. Hillerborg, M. Modeer, P.E. Peterson, Analysis of crack formation and crack growth in concrete by means of fracture mechanics and finite elements, Cem. Concr. Res. 6 (6) (1976) 773–782.

[22] C. Larive, Apport combinés de l'alcali-réaction et des ses effets mécaniques, D.Ing. thesis, Ecole Nationale des Ponts et Chaussées, Marne-la-Vallée, France, 1997 (in French).

[23] M. Pigeon, P. Plante, R. Pleau, N, Banthia, Influence of soluble alkalis on the production and stability of the air-void system in superplasticized and nonsuperplasticized concrete, ACI Mater. J. 89 (1) (1992) 24–31.

[24] M. Prezzi, P.J. Monteiro, G. Sposito, The alkali–silica reaction: Part I. Use of double-layer theory to explain the behavior of reaction-product gels, ACI Mater. J. 94 (1) (1997) 10–17.

[25] J.G. Rots, J. Blaauwendraad, Crack models for concrete: discrete or smeared? Fixed, multi-directional or rotating? Heron 34 (1) (1989).

[26] A. Shayan, Prediction of alkali reactivity of some Australian aggregates and correlation with service performance, ACI Mater. J. 89 (1) (1992) 13–23.

[27] D. Stark, Alkali–silica reaction and its effects on concrete, Proceedings of the Second International Conference on Alkali–Aggregate Reactions in Hydroelectric Plants and Dams, USCOLD, Chatanooga, Tennessee, 1995, pp. 9–18.

[28] F.-J. Ulm, O. Coussy, L. Kefei, C. Larive, Thermo-chemo-mechanics of ASR expansion in concrete structures, J. Eng. Mech. 126 (3) (1999) 233–242.

[29] M. Veilleux, Hydro-Québec's experience using deep slot cutting to rehabilitate concrete gravity dams affected by alkali–aggregate reaction, Proceedings of the Second International Conference on Alkali–aggregate Reactions in Hydroelectric Plants and Dams, USCOLD, Chatanooga, Tennessee, 1995, pp. 221–235.